




Intelligent Single-Cavity Dual-Comb Source With Fast Locking

Guoqing Pu , Runmin Liu, Chao Luo , Youjian Song , *Senior Member, IEEE*, Huan Mu, Weisheng Hu , *Member, IEEE*, Minglie Hu , and Lilin Yi 

Abstract—Dual-comb source (DCS) generation occupies the central position to the versatility of dual-comb applications. The single-cavity-based DCS generation is an emerging technology which provides superior mutual coherence between the two combs by sharing one laser cavity, therefore sophisticated active stabilization approaches are not necessary. However, the condition for starting and stabilizing dual-comb mode-locking in a single cavity is critical which hinder this technology towards practical applications. To resolve the bottleneck, we experimentally demonstrate the first intelligent single-cavity DCS by combining the real-time intelligent control module with the memory-aided intelligent searching algorithm. Given a tremendous six-dimensional parametric space, the intelligent DCS can operate under the dual-comb regime from a continuous wave state within a mean time of only 2.48 seconds. The dual-comb mode-locking state can be recovered automatically after interruption. The long-term stability of the intelligent DCS is validated as well through a 12-hour test in an open environment.

Index Terms—Dual-color dual-comb source, intelligent feedback control, memory-aided intelligent searching.

I. INTRODUCTION

OPTICAL frequency combs based on mode-locked lasers have revolutionized optical frequency metrology and a number of high-precision applications. In particular, a dual-comb configuration has attracted wide attention in recent years. With inherent optical asynchronous sampling, dual-comb technology allows high-resolution, high-sensitivity, and fast measurements in absolute ranging [1] and molecular spectroscopy [2], thereby extending its usage in microscopy [3], hyperspectral imaging [4], and holography [5]. Dual-comb source (DCS)

generation holds special appeal among the laser community due to its vital role in dual-comb applications. Typically, DCS generation requires phase-locking two independent mode-locked lasers so as to establish mutual coherence between the combs. Complex, bulky, and expensive laser locking systems are indispensable [1], [2], [3], [6]. The electro-optic modulation-based DCS generation is confined in applications due to the limited combs [4], [5], [7] and the micro-resonator to generate DCS is demanding on the component manufacturing process [8]. DCS generation from a single laser cavity by incorporating bidirectional [9], [10], [11], [12], [13], dual-polarization [14], [15], [16], [17], and dual-color [18], [19], [20], [21], [22] mechanisms becomes a promising alternative in recent years. The mutual coherence is passively maintained due to common-mode noise cancellation in a shared laser cavity. Moreover, the dual-comb configuration is significantly simplified.

However, it is a challenging task to establish the dual-comb regime and maintain it during operation. A material-based saturable absorber is used to assist dual-color DCS generation in a single cavity while intra-cavity polarization tuning is inevitable [18], [19], [20], [21], [22], and the same situation is found in the single-cavity-based dual-polarization DCS generation [15], [16], [17] and bidirectional DCS generation [9], [10], [12], [13]. The all-polarization-maintaining bidirectional single-cavity-based DCS partially resolve this problem, but careful cavity loss control in each direction is required so as to protect two independent saturable absorbers from damage and to balance the gain for two combs [11]. Besides, two combs generated through the partial-split bidirectional mechanism inherently do not share the entire cavity which may reduce the mutual coherence [11], [12]. Overall, the single-cavity-based DCS generation always relies on manual interference including critical intra-cavity polarization tuning [9], [10], [12], [13], [15], [16], [17], [18], [19], [20], [21], [22] and intra-cavity loss control [11], and the mode-locking is vulnerable to environmental disturbances [23], therefore limiting the practical applications of this technology.

To resolve the dilemma of the single-cavity-based DCS generation, we propose and experimentally demonstrate the first intelligent single-cavity DCS to ensure the laser fast locking on the dual-comb regime without manual interference. The proposed single-cavity DCS incorporates the dual-color mechanism, which is achieved through birefringent filtering dominated by a piece of polarization-maintaining fiber (PMF) with the dedicated-designed length inside the cavity. The intelligent DCS generation relies on real-time polarization tuning through

Manuscript received 31 March 2022; revised 27 October 2022; accepted 3 November 2022. Date of publication 8 November 2022; date of current version 15 January 2023. This work was supported by the National Natural Science Foundation of China under Grants 62025503 and 61827821. (Guoqing Pu and Runmin Liu contributed equally to this work.) (Corresponding author: Lilin Yi.)

Guoqing Pu, Chao Luo, Weisheng Hu, and Lilin Yi are with the State Key Lab of Advanced Communication Systems and Networks, School of Electronic Information and Electrical Engineering, Shanghai Jiao Tong University, Shanghai 200240, China (e-mail: teddyghf1994@sjtu.edu.cn; luochao@sjtu.edu.cn; wshu@sjtu.edu.cn; lilinyi@sjtu.edu.cn).

Runmin Liu, Youjian Song, and Minglie Hu are with the Ultrafast Laser Laboratory, Key Laboratory of Opto-electronic Information Science and Technology of Ministry of Education, College of Precision Instruments and Opto-electronics Engineering, Tianjin University, Tianjin 300072, China (e-mail: liurunmin@tju.edu.cn; yjsong@tju.edu.cn; huminglie@tju.edu.cn).

Huan Mu is with the R&D Center, AIOPTICS Company Limited, Shanghai 200240, China (e-mail: tony.mu@aioptics.cn).

Color versions of one or more figures in this article are available at <https://doi.org/10.1109/JLT.2022.3220258>.

Digital Object Identifier 10.1109/JLT.2022.3220258

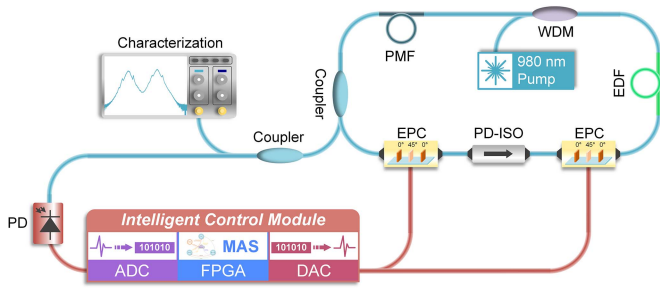


Fig. 1. The experimental setup of the intelligent single-cavity DCS.

two electric polarization controllers (EPCs) and an intelligent control module (ICM). The proposed memory-aided intelligent searching (MAIS) algorithm running inside the ICM can quickly locate the solution corresponding to the dual-color dual-comb regime in a tremendous six-dimensional parametric space, driving the laser from a continuous wave state to the dual-color dual-comb regime within a mean time of only 2.48 seconds. Further, 12-hour running tests of different algorithms in an open environment are performed and MAIS manifests the best robustness against the detachments (i.e., the laser loses the dual-color dual-comb regime) mainly induced by the environmental disturbances. Widespread high-precision metrological and spectroscopic applications based on this low-cost, compact, portable, and all-fiber intelligent DCS can be expected in the near future.

II. PRINCIPLES

A. Experimental Setup of the Intelligent DCS

Fig. 1 shows the experimental setup of the intelligent DCS consisting of the optical ring cavity, the ICM, and the characterization system. In the optical ring cavity, a polarization-dependent isolator (PD-ISO) sandwiched by two EPCs form the typical nonlinear-polarization-evolution mechanism for mode-locking. The electric-optic crystal-based EPC driven by three channels of DC voltages can produce an arbitrary polarization state around the Poincaré sphere within 10 μ s. To generate the dual-color DCS, a 16-cm PMF is used to introduce birefringent filtering [24]. The gain medium is a 40-cm erbium-doped fiber (EDF), which is pumped by a 980-nm laser via a wavelength division multiplexer (WDM). Nearly 90% of energy is retained inside the cavity, the rest serves as inputs for characterization and feedback through the coupler outside the cavity. The ICM supporting the real-time feedback control includes an analog-to-digital converter (ADC), a field-programmable gate array (FPGA), and 6 digital-to-analog converters (DACs).

B. Discrimination of the Dual-Color Dual-Comb Regime

To realize the intelligent DCS, it is imperative for the algorithm to discriminate the dual-comb regime accurately. Due to the repetition rate difference of the two combs of the dual-comb regime, RF spectra-based discrimination seems a good choice. However, the repetition rate difference is very small.

Therefore, a long-term single temporal acquisition is required to tell such a small difference in RF frequency domain but the long-term single temporal acquisition is intolerable for the real-time feedback control. For the dual-color DCS, the optical spectrum is featured with two separate mode-locked spectra. With time stretch-dispersive Fourier transform (TS-DFT) [25], [26] real-time spectral discrimination of the dual-color dual-comb regime looks plausible. However, the temporal asynchronization between two pulse trains due to the small repetition rate difference impedes the effective extraction of real-time spectra. With an optical coupler to split two wavelengths, TS-DFT based the dual-color dual-comb regime discrimination can be achieved by using two analog-to-digital converters (ADCs) to sample the real-time spectra separately. Thus, the complexities of both the experiment setup and the circuit design increase.

Temporal pulse count offers a straightforward solution although it also suffers from the temporal asynchronization. Nevertheless, pulse count is simple and requires little information on the pulse shape. Here, the temporal asynchronization problem can be resolved by multiple sampling on the output. Note that the second-order harmonic mode-locking regime has the identical pulse count as the dual-color dual-comb regime, while the pulses of harmonic mode-locking state are equally distributed. Therefore, the second-order harmonic mode-locking regime can be identified and filtered through judging on the inter-pulse margin in the multiple sampling process. The pulse count method cannot identify multiple tightly bounded solitons at either wavelength. However, the bound state can be detected from the modulations in optical spectrum and eliminated by decreasing pump power. The proposed discrimination of the dual-color dual-comb regime is validated well in the experiment.

C. Principles of MAIS

As Fig. 2 shows, MAIS is an algorithmic frame, where the optimization algorithms and the memory storing the historical empirical solutions, i.e., the control voltages of the EPCs, are bonded seamlessly to accelerate the searching phase. The memory allows basic operations including query and saving. Moreover, the memory supports dynamic updates, i.e., the stored solutions are updated cyclically. When the environment changes, the memory performs self-updating with the assistance of optimization algorithms thereby endowing MAIS with the strong robustness against environment vibrations.

Laser optimization is a complex and tough task, where multi-parameter control is usually required thereby forming a high-dimensional parametric space [26], [27], [28], [29], [30]. Intelligent algorithms can accelerate the optimization process and locate a better setting point than relying on manual tuning. Recently, several experimental studies prove that genetic algorithm (GA), a global optimization algorithm inspired by the theory of evolution [31], is a good choice in intelligent mode-locking [26], [27], [28], [29]. Here, GA is selected as the main search algorithm. However, using GA alone as the searching algorithm results in extremely large time consumption due to the tremendous six-dimensional parametric space, therefore MAIS is proposed to accelerate the searching phase.

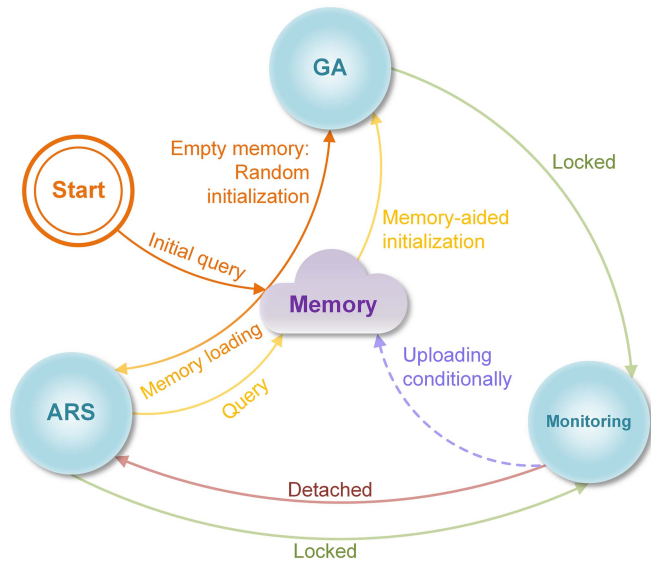


Fig. 2. The principles of MAIS. GA is the main search engine and ARS is to deal with detachments of DCS and fast boot. MAIS is trapped in the discrimination-based monitoring after the dual-comb regime is found. The dynamic memory allows basic operations including query, loading and uploading.

A pure temporal fitness function of the search algorithms is designed, as indicated in (1) shown at the bottom of this page. The first term of the fitness function is the scaled sum of the pulse amplitude, where C_{ideal} denotes the ideal pulse count for the dual-comb regime, C_{real} is the real pulse count based on the current waveform, A_i denotes the amplitude of the i -th pulse. The following term is a punishing term of the pulse count error and α is the weight. The third term is another punishing term about the periodicity, where P_k represents the position for the k -th pulse, S_{rep} is the number of sampling points in one period and β is the weight. The last term is an extra bonus term calculating the difference between the inter-pulse margin and the number of sampling points in a second-harmonic period, and γ is the weight. For the second-order harmonic mode-locking regime, the last term is close to 0. Therefore, the last term is designed to ensure that the dual-comb regime scores a larger fitness than the second-order harmonic mode-locking regime. In our fitness function, α , β and γ are 4, 0.3 and 0.005 respectively. Note that the pulse used to calculate the last two terms is randomly selected.

On the path to dual-color dual-comb source generation through manual polarization tuning, it usually runs into a one-side fundamental mode-locking regime, i.e., one side has the board spectrum, and the other side has strong continuous wave components. Then, the dual-color dual-comb regime is bred from the one-side fundamental mode-locking regime via more precise polarization tuning. Given the empirical experiences, the fitness of the fundamental mode-locking regime should be treated with care. As shown in the bottom line of (1), to give the fundamental mode-locking regime a larger fitness, the punishing term of the pulse count error is cancelled. Besides, two sets of temporal pulse trains overlap periodically due to the temporal asynchronization, thereby manifesting a quite similar temporal waveform to the fundamental mode-locking regime.

The overlapped dual-comb regime can also score a decent fitness and, therefore, it will not be filtered during optimization.

An initial query is firstly performed to ascertain whether the memory is empty. GA will be randomly initialized if the memory is empty. Otherwise, the algorithm turns to the advanced Rosenbrock search (ARS), a non-computation-intensive local optimization algorithm used for intelligent mode-locking [30]. Combining the dynamics memory scheme with ARS, fast locating on the dual-comb regime becomes possible. To this end, ARS will try each empirical solution inside the memory reversely. The step of initializing ARS with an empirical solution is termed memory loading. Before memory loading, a query is raised to check whether there are un-tested empirical solutions left inside the memory. If ARS successfully guides the laser to the dual-comb regime, then the algorithm enters the dual-comb regime discrimination-based monitoring. However, when the ARS fails, a memory-aided initialization will be carried out for GA, where the latest empirical solutions inside the memory are selected as the initial population.

By enlarging the fitness, GA gradually guides the laser to the dual-comb regime. Combining with the temporal dual-comb regime discrimination, GA is terminated immediately once the dual-comb regime emerges. Then, the algorithm enters the dual-comb regime discrimination-based monitoring, which allows the algorithm to detect detachments in time. Once a detachment is detected, the algorithm will upload the current solution to the memory conditionally. Concretely, several well-designed judgments are required before the current solution is uploaded to the memory. First, to ensure the current solution is relatively good, the stabilization time of the current solution should be longer than 30 s. The stabilization time is defined as the time that the laser keeps operating on the dual-comb regime and it is timed by a global timer with a resolution of ~ 3 ns. Then, if the memory is not empty, the algorithm will evaluate the difference between the current solution and the latest empirical solution via Euclidean distance calculation. When the Euclidean distance between the current solution and the latest empirical solution surpasses the pre-set threshold, the current solution will be considered as a new different solution and uploaded to the memory. Afterwards, the algorithm turns to ARS again thereby forming a closed-loop algorithmic frame.

III. RESULTS AND DISCUSSION

The dual-color dual-comb regime found by MAIS is shown in Fig. 3. The optical spectrum in Fig. 3(a) indicates a dual-color dual-comb regime. Due to the birefringent filtering dominated by the PMF, there is a separation of 33.9 nm between two central wavelengths. The theoretic wavelength separation is ~ 30 nm calculated by (2), where λ is the central wavelength, L_{PMF} is the length of the PMF and Δn is the birefringent coefficient of the PMF. The RF spectrum in Fig. 3(b) shows that the repetition rate is ~ 10.42 MHz and the repetition rate difference is 1.05 kHz. Because the laser cavity is mainly composed of standard-single-mode fiber with anomalous dispersion, the red sideband of the dual-comb regime propagates slightly slower than the

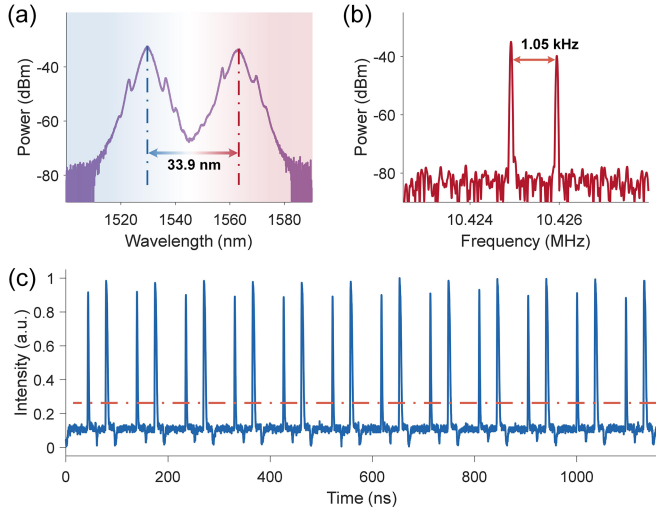


Fig. 3. The dual-color dual-comb regime found by MAIS. (a) The optical spectrum has two bands with a separation of 33.9 nm. (b) The repetition rate is ~ 10.42 MHz and the repetition difference is 1.05 kHz. (c) The temporal waveform consists of two pulse trains; the dashed line is the count threshold.

blue one. Therefore, the red sideband corresponds an optical frequency comb with a smaller free spectral range (FSR) of ~ 10.425 MHz and the blue sideband corresponds an optical frequency comb with a larger FSR of ~ 10.426 MHz. The typical temporal waveform of the dual-color dual-comb regime is shown in Fig. 3(c).

$$\Delta\lambda = \frac{\lambda^2}{L_{PMF} \cdot \Delta n} \quad (2)$$

Time consumption performance is tested through an FPGA-internal timer with a resolution of 3.3 ns. Fig. 4(a) shows the time consumption over 50 boot (i.e., from free-running state to the dual-color dual-comb regime) of both MAIS and GA only. In the searching phase, the control values of both EPCs refresh nearly every millisecond. One iteration of GA costs ~ 100 ms averagely, and the number of iterations required to find the dual-comb regime is dependent to the random initial population generation and the surrounding environment including thermal and mechanical influences. As a result, the mean time of MAIS is only 2.48 seconds, which is ~ 50 times short than GA, and the standard deviation of MAIS is ~ 8 times smaller than GA. As expected, for MAIS, the initial several boots demand comparable time as GA due to the empty memory in the beginning. MAIS relies on GA to search the dual-color dual-comb regime in the early stage. As the number of empirical solutions inside the memory grows, ARS becomes the main force in searching

the dual-color dual-comb regime thereby substantially reducing the booting time. The time consumption test experimentally validates the performance enhancement introduced by MAIS. The fitness map shown in Fig. 4(b) is obtained through scanning over two channels of one EPC and keeping the rest four channels fixed. The two points in dark blue own the maximum fitness corresponding to the dual-color dual-comb regime, proving the solution space is very small for the dual-color dual-comb regime and it is extremely difficult to achieve by manual tuning. Because of the special design in the fitness function for the fundamental mode-locking regime, the platform in blue with larger fitness is the aggregation of the points corresponding to the fundamental mode-locking regime. Due to the nonlinear polarization evolution inside the laser cavity, the fitness distribution in Fig. 4(b) is aperiodic as the scanning ranges of the two channels surpass 2π .

Fig. 5 shows the results of 12-hour optical spectrum monitoring tests in an open environment. The spectrum is updated every 4.5 seconds. In free-running case, the laser keeps operating under the dual-color dual-comb regime for ~ 3 hours till the instabilities come into play. After several self-relocking, the laser ultimately turns into a fundamental mode-locking regime with a strong continuous wave component as shown in the white box of Fig. 5(a). The result of using GA for both boot and detachments recovery is shown in Fig. 5(b). Note that GA starts from the last generation rather than a random generation when dealing with detachments. GA is unable to deal with detachments in a short time thereby existing many gaps during 12 hours. For comparison, the algorithmic combination of GA and ARS (GA-ARS) is tested, where the boot is managed by GA alone and detachments recovery is taken care of by both ARS and GA. ARS is firstly launched when encountering detachments. If ARS fails, GA will be re-run from the last generation to recover from detachments. The algorithmic combination manifests a substantial performance improvement as shown in Fig. 5(c). However, due to the lack of the seamless bond between the optimization algorithms and the memory storing the historical empirical solutions, detachments recovery can be time-costly. Therefore, a distinct gap and instabilities are observed in Fig. 5(c). Fig. 5(d) shows the laser governed by MAIS almost continuously operate under the dual-color dual-comb regime for 12 hours.

The stability of the laser is not only related to environmental disturbances, but also affected by the linear loss in the cavity, especially the nonlinear-polarization-evolution mode-locking structure. The linear loss of the cavity is measured to be about 3 dB, substantially contributed by EPCs with a loss of ~ 1.2 dB/PC. However, the instability of dual-color dual-comb regime manifests the decent performance of MAIS. Because the fitness function and discrimination are designed based on pure temporal information, the optical spectrum of the dual-color dual-comb

$$F = \begin{cases} \frac{\sum_{i=1}^{C_{real}} A_i}{C_{ideal}} - \alpha |C_{real} - C_{ideal}| - \beta |(P_{k+2} - P_k) - S_{rep}| + \gamma \left| (P_{k+1} - P_k) - \left\lfloor \frac{S_{rep}}{2} \right\rfloor \right|, & |C_{real} - \left\lfloor \frac{C_{ideal}}{2} \right\rfloor| > 0.1 \left\lfloor \frac{C_{ideal}}{2} \right\rfloor \\ \frac{\sum_{i=1}^{C_{real}} A_i}{C_{ideal}} - \beta |(P_{k+2} - P_k) - S_{rep}| + \gamma \left| (P_{k+1} - P_k) - \left\lfloor \frac{S_{rep}}{2} \right\rfloor \right|, & \text{otherwise} \end{cases} \quad (1)$$

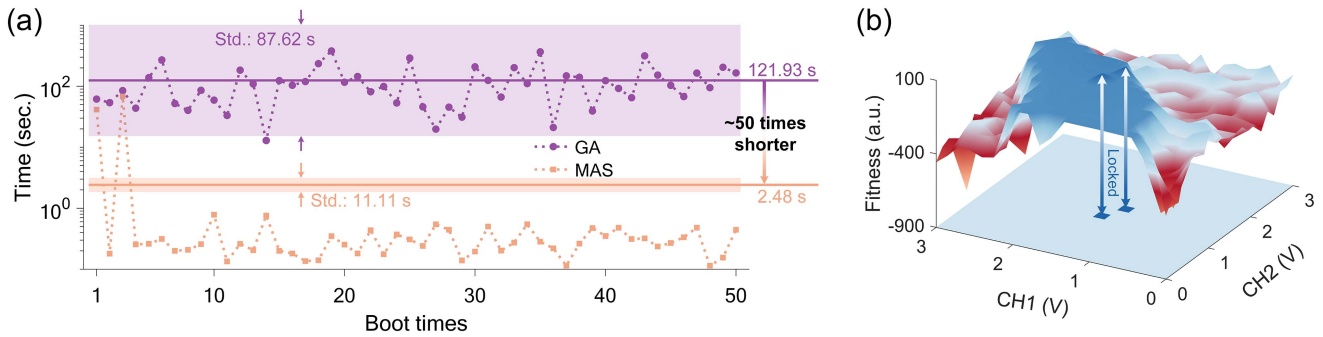


Fig. 4. (a) Time consumption over 50 boot of GA and MAIS. With MAIS, the laser can operate under the dual-color dual-comb regime from the free-running state within a mean time of 2.48 seconds, which is ~ 50 times faster than using GA. (b) The fitness map obtained through scanning over two channels of one EPC (the rest four channels are fixed). Only two points with the maximum fitness correspond to the dual-color dual-comb regime.

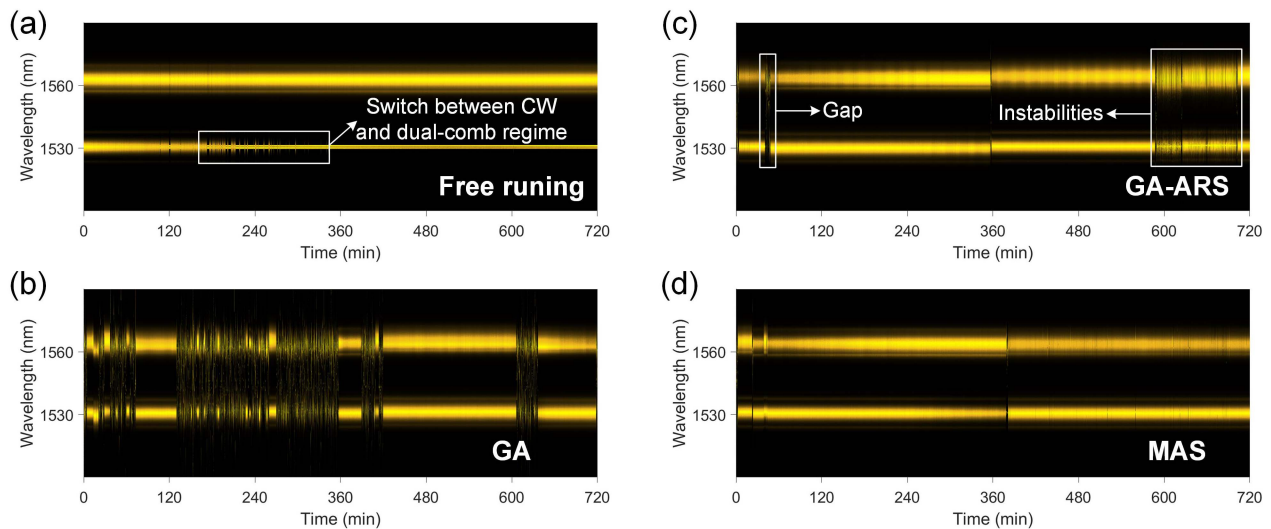


Fig. 5. 12-hour optical spectrum monitoring tests. (a) The laser keeps operating under the dual-color dual-comb regime for ~ 3 hours in free-running case. (b) Many gaps exist when using GA for both boot and detachments recovery. (c) The algorithmic combination of GA and ARS (GA-ARS) substantially improve the performance while a distinct gap and instabilities are still observed. (d) The laser governed by MAIS almost continuously operate under the dual-color dual-comb regime for 12 hours.

regime found by algorithms may vary slightly from time to time, which can be resolved through introducing spectral information to the algorithm.

IV. CONCLUSION

An intelligent single-cavity DCS incorporating a dual-color mechanism is realized via the combination of the real-time ICM, the dedicatedly-designed discrimination of the dual-color dual-comb regime, and the algorithmic frame, MAIS. Given a tremendous six-dimension parametric space with extremely small solution space, MAIS can locate a desired solution in a mean time of only 2.48 seconds due to the unique seamless bond between the memory storing the empirical solutions and ARS thereby accelerating the searching phase. Further, under the governing of MAIS, the intelligent DCS manifests as a stable DCS working for the long term. Compared to the dual-cavity-based DCS generation, the intelligent DCS substantially simplified the

setup by using a single-cavity thereby saving the bulky synchronization systems. The intelligent DCS is undoubtedly easier to use and more stable than the traditional single-cavity DCS. The feedback architecture, the proposed MAIS, and discrimination of the dual-comb regime also suit the single-cavity DCS incorporating bidirectional and dual-polarization mechanisms with moderate modifications.

REFERENCES

- [1] I. Coddington, W. C. Swann, L. Nenadovic, and N. R. Newbury, "Rapid and precise absolute distance measurements at long range," *Nature Photon.*, vol. 3, no. 6, pp. 351–356, 2009.
- [2] I. Coddington, N. R. Newbury, and W. C. Swann, "Dual-comb spectroscopy," *Optica*, vol. 3, no. 4, pp. 414–426, 2016.
- [3] E. Hase et al., "Scan-less confocal phase imaging based on dual-comb microscopy," *Optica*, vol. 5, no. 5, pp. 634–643, 2018.
- [4] P. M. Mateos, F. U. Khan, and O. E. B. Manrique, "Direct hyperspectral dual-comb imaging," *Optica*, vol. 7, no. 3, pp. 199–202, 2020.

- [5] E. Vicentini, Z. Wang, K. V. Gasse, T. W. Hänsch, and N. Picqué, "Dual-comb hyperspectral digital holography," *Nature Photon.*, vol. 15, no. 12, pp. 890–894, 2021.
- [6] I. Coddington, W. C. Swann, and N. R. Newbury, "Coherent multiheterodyne spectroscopy using stabilized optical frequency combs," *Phys. Rev. Lett.*, vol. 100, no. 1, 2008, Art. no. 013902.
- [7] G. Millot et al., "Frequency-agile dual-comb spectroscopy," *Nature Photon.*, vol. 10, no. 1, pp. 27–30, 2016.
- [8] M.-G. Suh, Q.-F. Yang, K. Y. Yang, X. Yi, and K. J. Vahala, "Microresonator soliton dual-comb spectroscopy," *Science*, vol. 354, no. 6312, pp. 600–603, 2016.
- [9] K. Kieu and M. Mansuripur, "All-fiber bidirectional passively mode-locked ring laser," *Opt. Lett.*, vol. 33, no. 1, pp. 64–66, 2008.
- [10] S. Mehravar, R. A. Norwood, N. Peyghambarian, and K. Kieu, "Real-time dual-comb spectroscopy with a free-running bidirectionally mode-locked fiber laser," *Appl. Phys. Lett.*, vol. 108, no. 23, 2016, Art. no. 231104.
- [11] S. Saito, M. Yamanaka, Y. Sakakibara, E. Omoda, H. Kataura, and N. Nishizawa, "All-polarization-maintaining Er-doped dual comb fiber laser using single-wall carbon nanotubes," *Opt. Exp.*, vol. 27, no. 13, pp. 17868–17875, 2019.
- [12] Y. Nakajima, Y. Hata, and K. Minoshima, "High-coherence ultra-broadband bidirectional dual-comb fiber laser," *Opt. Exp.*, vol. 27, no. 5, pp. 5931–5944, 2019.
- [13] B. Li et al., "Bidirectional mode-locked all-normal dispersion fiber laser," *Optica*, vol. 7, no. 8, pp. 961–964, 2020.
- [14] S. M. Link et al., "Dual-comb modelocked laser," *Opt. Exp.*, vol. 23, no. 5, pp. 5521–5531, 2015.
- [15] A. E. Akosman and M. Y. Sander, "Dual comb generation from a mode-locked fiber laser with orthogonally polarized interlaced pulses," *Opt. Exp.*, vol. 25, no. 16, pp. 18592–18602, 2017.
- [16] X. Zhao, T. Li, Y. Liu, Q. Li, and Z. Zheng, "Polarization-multiplexed, dual-comb all-fiber mode-locked laser," *Photon. Res.*, vol. 6, no. 9, pp. 853–857, 2018.
- [17] Y. Nakajima, Y. Hata, and K. Minoshima, "All-polarization-maintaining, polarization-multiplexed, dual-comb fiber laser with a nonlinear amplifying loop mirror," *Opt. Exp.*, vol. 27, no. 10, pp. 14648–14656, 2019.
- [18] X. Zhao et al., "Picometer-resolution dual-comb spectroscopy with a free-running fiber laser," *Opt. Exp.*, vol. 24, no. 19, pp. 21833–21845, 2016.
- [19] G. Hu, Y. Pan, X. Zhao, S. Yin, M. Zhang, and Z. Zheng, "Asynchronous and synchronous dual-wavelength pulse generation in a passively mode-locked fiber laser with a mode-locker," *Opt. Lett.*, vol. 42, no. 23, pp. 4942–4945, 2017.
- [20] R. Liao, Y. Song, W. Liu, H. Shi, L. Chai, and M. Hu, "Dual-comb spectroscopy with a single free-running thulium-doped fiber laser," *Opt. Exp.*, vol. 26, no. 8, pp. 11046–11054, 2018.
- [21] R. Li et al., "All-polarization-maintaining dual-wavelength mode-locked fiber laser based on Sagnac loop filter," *Opt. Exp.*, vol. 26, no. 22, pp. 28302–28311, 2018.
- [22] J. Fellinger, G. Winkler, A. S. Mayer, L. R. Steidle, and O. H. Heckl, "Tunable dual-color operation of yb: Fiber laser via mechanical spectral subdivision," *Opt. Exp.*, vol. 27, no. 4, pp. 5478–5486, 2019.
- [23] M. Karlsson, J. Brentel, and P. A. Andrekson, "Long-term measurement of PMD and polarization drift in installed fibers," *J. Lightw. Technol.*, vol. 18, no. 7, pp. 941–951, Jul. 2000.
- [24] A. Khanolkar, X. Ge, and A. Chong, "All-normal dispersion fiber laser with a bandwidth tunable fiber-based spectral filter," *Opt. Lett.*, vol. 45, no. 16, pp. 4555–4558, 2020.
- [25] G. Herink, B. Jalali, C. Ropers, and D. R. Solli, "Resolving the build-up of femtosecond mode-locking with single-shot spectroscopy at 90 MHz frame rate," *Nature Photon.*, vol. 10, no. 5, pp. 321–326, 2016.
- [26] G. Pu, L. Yi, L. Zhang, C. Luo, Z. Li, and W. Hu, "Intelligent control of mode-locked femtosecond pulses by time-stretch-assisted real-time spectral analysis," *Light.: Sci. Appl.*, vol. 9, no. 1, pp. 1–8, 2020.
- [27] U. Andral, R. S. Fodil, F. Amrani, F. Billard, E. Hertz, and P. Grelu, "Fiber laser mode locked through an evolutionary algorithm," *Optica*, vol. 2, no. 4, pp. 275–278, 2015.
- [28] R. I. Woodward and E. J. R. Kelleher, "Towards 'smart lasers': Self-optimisation of an ultrafast pulse source using a genetic algorithm," *Sci. Rep.*, vol. 6, no. 1, pp. 1–9, 2016.
- [29] R. I. Woodward and E. J. R. Kelleher, "Genetic algorithm-based control of birefringent filtering for self-tuning, self-pulsing fiber lasers," *Opt. Lett.*, vol. 42, no. 15, pp. 2952–2955, 2017.
- [30] G. Pu, L. Yi, L. Zhang, and W. Hu, "Intelligent programmable mode-locked fiber laser with a human-like algorithm," *Optica*, vol. 6, no. 3, pp. 362–369, 2019.
- [31] J. H. Holland, "Genetic algorithms," *Sci. Amer.*, vol. 267, no. 1, pp. 66–73, 1992.